

Article

A Decision for Throughput Optimization in UAV-Enabled Emergency Outdoor–Indoor Fairness Communication

Zinan Guo ¹, Bo Hu ^{1,*} and Shanzhi Chen ²

¹ State Key Laboratory of Networking and Switching Technology, Beijing University of Posts and Telecommunications, Beijing 100876, China

² State Key Lab of Wireless Mobile Communication, China Academy of Telecommunication Technology, Beijing 100049, China

* Correspondence: hubo@bupt.edu.cn

Abstract: This paper investigates the throughput optimization strategy in an unmanned aerial vehicle (UAV)-enabled emergency outdoor–indoor fairness communication scenario, with the UAV as a mobile relay station in the air, to provide outdoor–indoor communication services for users inside buildings. The occurrence of severe signal fading caused by outdoor transmission loss through wall loss as well as indoor transmission loss when the UAV forwards the information to the indoor users reduces the channel gain and degrades the system downlink throughput. To improve the downlink throughput of the system and ensure communication fairness for indoor users, we designed a joint UAV location deployment and resource allocation (JLRO) algorithm that optimized UAV three-dimensional (3D) deployment location, power and bandwidth resource allocation. The simulation results demonstrate the convergence and validity of the proposed JLRO algorithm, as well as its superiority compared to benchmark algorithms.

Keywords: UAV; throughput; outdoor–indoor transmission; fairness; LOS-NLOS



Citation: Guo, Z.; Hu, B.; Chen, S. A Decision for Throughput Optimization in UAV-Enabled Emergency Outdoor–Indoor Fairness Communication. *Drones* **2023**, *7*, 460. <https://doi.org/10.3390/drones7070460>

Academic Editor: Riadh Dhaou

Received: 30 May 2023

Revised: 4 July 2023

Accepted: 9 July 2023

Published: 11 July 2023



Copyright: © 2023 by the authors. Licensee MDPI, Basel, Switzerland. This article is an open access article distributed under the terms and conditions of the Creative Commons Attribution (CC BY) license (<https://creativecommons.org/licenses/by/4.0/>).

1. Introduction

Previously, unmanned aerial vehicles (UAVs) have been widely used in civil fields [1]. With the development of millimeter-wave/terahertz technology, UAVs can use this technology for sensing, communication and control scheduling [2]. In emergencies such as natural disasters, the communication infrastructure may not work properly due to damage or other reasons. At this time, the communication network will face paralysis and other problems. Moreover, the response time of the infrastructure is long, and the emergency area may be in a state of loss of contact for a period of time, which is very detrimental to rescue operations [3]. With the advantage of flexible flight, UAVs can establish the first emergency communication networks for disaster areas [4]. The transmission of videos and images will be beneficial for rescue operations. For multimedia data, the transmission is significantly different from traditional communication data, which has a high data volume and requires a high throughput system for transmission [5]. So, it is very important to study the throughput of outdoor–indoor communication systems built by UAVs. However, so far, compared with outdoor, there has been less research on the establishment of communication systems for indoor users by UAVs.

In [6], the author used the Manhattan city model to fit and analyze the measured data and obtained the air-to-ground (ATG) model. In the process of building the model, the author considered the probability of the line-of-sight (LOS) and the non-line-of-sight (NLOS). The height of UAVs was optimized by finding the balance between energy savings and maximum coverage. This model has been cited by a large number of scholars. S. ur Rahman et al. in [7] jointly optimized the three-dimensional (3D) deployment locations of multiple UAVs and the control strategy of UAVs to maximize the system throughput. Wu Q et al. in [8] optimized the flight angle, radius and speed of the UAV combined

with bandwidth allocation technology, and achieved the maximum coverage of users on the premise of meeting the minimum throughput. J. Miao et al. in [9] and J.H. Lee et al. in [10] jointly optimized the transmission power, transmission time and trajectory to ensure the maximum throughput of the system. The article [11] proposed a collaborative design scheme for quality of service (QoS)-oriented sensor communication control (SCC) of UAVs. The stability and location service performance of the UAV were analyzed by building the UAV status and control model. The problem of minimizing the amount of data transmitted by optimizing perceptual scheduling and block length allocation while meeting the location accuracy requirements of each user was further investigated. The article [12] minimizes the energy of data upload networks by optimizing the trajectory of UAVs and sensor power consumption.

The above research on the throughput of UAV communication systems is aimed at outdoor users. The models they use are ATG models or are modified on the basis of ATG models. However, these models are difficult to directly apply to the outdoor–indoor communication system because the signal must not be a LOS link when it is transmitted from the outdoor to the indoor. That is to say, because of the existence of the wall, the LOS probability of the ATG model in the outdoor–indoor communication system is zero. In addition, in the process of signal transmission, there is also the problem of the wall material and thickness inducing different through-wall losses. Moreover, the calculation of the transmission loss of signal indoors is also different from that outdoors.

In [13], the author proposed a loss model for outdoor–indoor communication. By optimizing the 3D location of a single UAV, comprehensive coverage of all indoor users was achieved. They considered two different coverage scenarios. One is that the UAV stays in the center of a wall in the building. If it can provide services to the farthest users, it can also provide services to other users. This method wastes a lot of resources but is fast to deploy. The other is to optimize the coordinates of the UAV according to user coordinates. This has high resource utilization but slow deployment. In [14], the author uses the main path of the signal transmission in [15] for reference to optimize the outdoor–indoor transmission loss model and realizes all indoor users with the minimum outage probability by optimizing the 3D deployment location and bandwidth resource allocation of multiple UAVs. In [16], J. Cui et al. further studied the scenario of a UAV building a communication system for mixed users. An “indoor-outdoor-iterative optimization” (IOI) deployment scheme was proposed to avoid the problem that mixed users cannot be normalized. By ensuring equal communication quality for all users, this scheme achieves the maximum coverage for mixed users. Although prior research has investigated the indoor–outdoor communication model for UAVs, it has not examined the throughput of an outdoor–indoor communication system.

In [17], Abhijit Bhowmick et al. consider the wireless powered communication network (WPCN) system supported by a UAV to serve a set of terrestrial users. They optimized the UAV's maneuverability through trajectory design and wireless resource allocation to maximize the throughput of the system. Meng Hua et al. studied UAV-assisted uplink/downlink networks in [18] to maximize the throughput of the system; they optimized the trajectory of the UAV, the communication scheduling and the transmission power of the UAV-access points/sensor nodes (AP/SN). In case of an emergency, in order to improve the rescue efficiency of indoor users, Junghwa Kang et al. [19] proposed an uplink network based on a full-duplex UAV under disaster conditions to improve the system throughput. Lifeng Xie et al. studied a kind of UAV in [20] that supports the dual-user interference channel of a WPCN. The goal was to maximize the system throughput by optimizing the UAV flight trajectory and resource allocation under the UAV flight speed limit, collision avoidance and energy constraints of Internet of Things (IoT) devices. In [21], Tianyu Liu et al. considered a multi-link relay system supported by UAVs, in which multiple sources communicate with their destinations simultaneously through multiple UAV relays and share the same spectrum. It is proposed that the minimum throughput of all links can be maximized by jointly optimizing the 3D trajectory of UAV repeaters and the transmission

power levels of the source and the UAV repeaters. However, these studies do not take into account the fairness of user communication.

In UAV-enabled emergency communication scenarios, the signals forwarded by the UAV relay to indoor users undergo three stages of loss: outdoor transmission loss, through-wall transmission loss and indoor transmission loss. These losses lead to a reduction in the user's received signal-to-noise ratio (SNR), which, in turn, diminishes the system's downlink throughput. In this paper, to enhance the efficiency of emergency scene rescue efforts, a scheme involving UAV 3D location deployment and resource allocation is examined with the objective of maximizing system throughput while ensuring communication fairness among users.

By jointly optimizing location deployment and the resource allocation of UAVs, this paper proposes using the JLRO algorithm to maximize the system throughput in this network. The proposed JLRO algorithm fully considers the information causality constraints and ensures the fairness of users. The rationality of the proposed JLRO algorithm can be explained as follows: since the transmission loss from the UAV to the indoor UE is directly affected by the UAV's location and power allocation, the UAV's location deployment and power allocation are considered to be jointly optimized via the proposed JLRO algorithm. In this way, the transmission loss from the UAV to the indoor UE can be reduced such that the channel gain is further improved. As a result, the indoor user's received SNR is further boosted, which increases the system's downlink throughput.

In UAV-enabled emergency communication scenarios, the UAV serves as a communication relay and establishes a two-hop communication link. The first hop is from the ground base station (BS) to the UAV, and the second hop is from the UAV to multiple indoor users. In the second-hop communication link, the signals forwarded by the UAV to the indoor users undergo three stages of loss: outdoor transmission loss, wall transmission loss and indoor transmission loss. These losses can lead to a decrease in the user's received SNR, which, in turn, reduces the system's downlink throughput. However, in emergency rescue communication scenarios, every user should benefit from the same communication quality.

In a two-hop link communication system, due to information causal constraints, the sum of the throughput of each link in the second hop is not greater than the throughput of the first hop link. Therefore, in order to maximize indoor users' communication throughput, it is necessary to maximize the sum of the throughput of each link in the second hop. The signal transmission loss is affected by the location and power allocation of the UAV and the bandwidth allocation of the two hops.

In this paper, a scheme involving 3D location deployment and resource allocation of UAVs is studied with the goal of maximizing the system throughput while ensuring fair communication among users. We propose a joint UAV location deployment and resource allocation (JLRO) algorithm to maximize the system throughput in the network. The proposed JLRO algorithm fully considers the constraints of information causality, ensuring user fairness.

The main contributions of this article are as follows:

- We consider the outdoor propagation model and the outdoor–indoor propagation model based on LOS and NLOS links and establish a hybrid communication model. The maximization of the UAV system throughput is quantified as a mathematical problem.
- Based on the UAV's location and resource (power and bandwidth) allocation, a JLRO algorithm is proposed to address the mathematical problem of throughput maximization. In order to solve the complex function with non-concave characteristics, we decompose the original function into location and resource allocation, and then iterate and converge them.
- The proposed JLRO algorithm converges within six iterations. This effectively maximizes system throughput while adhering to the dual constraints of user fairness and information causality.

In Section 2, the throughput optimization of a UAV communication system based on user fairness is proposed. Section 3 expatiates a JLRO algorithm for the UAV's location and

bandwidth and power allocation. Section 4 presents the simulation in detail, and Section 5 presents the conclusions of this paper.

2. System Model and Problem Formulation

In cases of emergencies such as natural disasters, communication infrastructure becomes out of service due to damage. UAVs can move freely in the air and can set up the first emergency communication systems for users after the earthquake occurs to ensure normal communication in the affected area. In this article, the network built by the undamaged ground base station and the new air emergency communication network are independent of each other, and the same frequency interference is not considered for the time being. In Figure 1a, a UAV establishes a two-hop relay link between indoor users and ground base stations to transmit base station information to users by acting as an air relay. Figure 1b shows a master transmission path plan when a base station transmits information to indoor users. In Figure 1b, $S(x_S, y_S, z_S)$ represents the coordinates of the signal transmitter, which, in this case, is the ground base station and is defined as the source node. $R(x_R, y_R, z_R)$ represents the coordinates of the relay, which, in this case, is the UAV. $D_i(x_i, y_i, z_i)$ represents the coordinates of a signal receiver, which, in this case, is an indoor user i , defined as a destination node. The number of users is indicated with n . It is assumed that the user's coordinates can be obtained or predicted [22], and the acquisition of user coordinates is not the focus of this study. $d_{S,R}$, d_{R,D_i} and d_i represent the linear distance between the BS and the UAV, the linear distance between the UAV and the exterior wall of the building, and the indoor transmission distance of the signal (the vertical distance from the user to the interior wall of the building), respectively. The unit of distance is meters (m). θ represents the elevation angle of a signal passing through the wall when the UAV communicates with the i -th indoor user. B is a building, and the length, width and height of B can be represented as x_B , y_B and z_B . In B , the floor height is set to 3 m. Users' communication equipment is generally at 1.5 m above the floor.

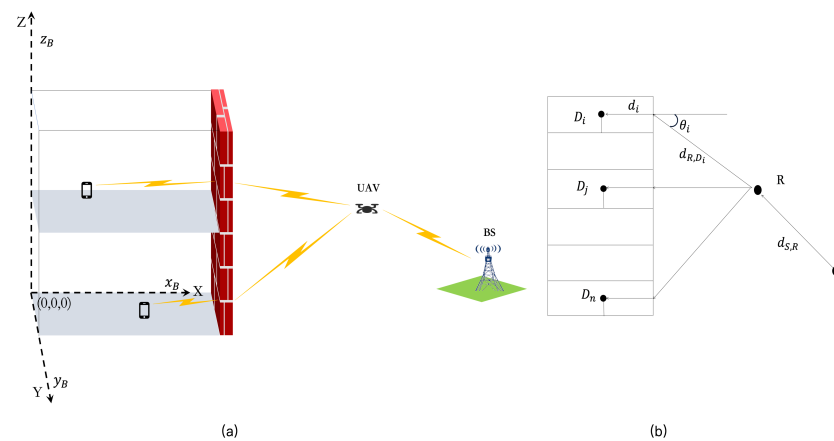


Figure 1. A UAV establishes a two-hop relay communication system for indoor users. (a) a UAV establishes a two-hop relay link between indoor users and ground base stations to transmit base station information to users by acting as an air relay; (b) a master transmission path plan when a base station transmits information to indoor users.

The signal transmission from the ground base station to the indoor user is a two-hop link. The first hop link refers to the transmission of signals from the ground base station to the UAV using the ATG communication model. The second hop link refers to the NLOS communication model used for the signal transmission from the UAV to indoor users. In terms of transmission loss, the first hop link and the second hop link are different. In the second hop link, the signal transmission loss mainly includes three parts: the path loss of the signal transmission outside the building, the path loss when the signal passes through

the building wall and the path loss when the signal is transmitted indoors. The unit of loss is db . The path loss model of the second hop link is mathematically quantified as:

$$PL_{2i} = PL_{Fi} + PL_{Bi} + PL_{Li}, \quad (1a)$$

$$PL_{Fi} = 20 \log_{10} \left(\frac{4\pi f d_{R,D_i}}{c} \right), \quad (1b)$$

$$PL_{Bi} = \beta_1 + \beta_2 (1 - \cos \theta_i)^2, \quad (1c)$$

$$PL_{Li} = \beta_3 d_i, \quad (1d)$$

where

$$d_{R,D_i} = \sqrt{(x_R - x_B)^2 + (y_R - y_i)^2 + (z_R - z_i)^2}, \quad (2a)$$

$$\cos \theta_i = \frac{x_R - x_B}{d_{R,D_i}}, \quad (2b)$$

$$d_i = x_B - x_i. \quad (2c)$$

In expression (1), PL_{2i} represents the second hop path loss of the i -th user, where PL_{Fi} represents the outdoor transmission loss of the i -th user in the second hop link. The outdoor transmission model uses a free path loss model because this path is an LOS link and the distance is very short. PL_{Bi} represents the wall transmission loss of the i -th user in the second hop link. PL_{Li} indicates the indoor transmission loss of the i -th user in the second hop link. c represents the speed of light, and $c = 3 * 10^8$. f represents the carrier frequency used for the signal. $\beta_1 = 14$, $\beta_2 = 15$, $\beta_3 = 0.5$. The above data and formulas are from the ITU standard [23].

The transmission speed of the i -th user in the second hop link is mathematically quantized as:

$$T_{2i} = B_{2i} \log_2 \left(1 + \frac{P_{2i} 10^{-\frac{PL_{2i}}{10}}}{B_{2i} N_0} \right). \quad (3)$$

P_{2i} and B_{2i} represent the power and bandwidth, respectively, allocated by the UAV to the i -th user in the second hop link. N_0 is the noise power spectral density.

In the first hop link, the total transmission loss is equal to the outdoor transmission loss and a widely used LOS probability-based transmission model is adopted. According to [6], the LOS probability of the first hop link is obtained as follows:

$$P_{LoS} = \frac{1}{1 + a_0 \exp[-b_0 (\frac{180}{\pi} \theta - a_0)]}. \quad (4)$$

a_0 and b_0 are environment-related constants, $\theta = \tan^{-1}(\frac{z_R - z_S}{d_H})$ is the elevation angle of the first hop link and $d_H = \sqrt{(x_R - x_S)^2 + (y_R - y_S)^2}$.

The channel of the first hop link is the ATG channel, except for the distance-based free space path loss; the ATG channel also suffers from the additional path loss that is dependent on the channel propagation condition. Assuming the LOS propagation condition, the total path loss of the first hop is $20 \log_{10}(\frac{4\pi f d_{S,R}}{c}) + \eta_{LoS}$, where η_{LoS} is the supplementary path loss for the LOS channel. Similarly, denote η_{NLoS} as the supplementary path loss for the NLOS channel, and the total path loss of the first hop under the NLOS channel is $20 \log_{10}(\frac{4\pi f d_{S,R}}{c}) + \eta_{NLoS}$. Consequently, the average path loss of the first hop link is provided by [6]:

$$\begin{aligned}
 PL &= P_{LoS}(20 \log_{10}(\frac{4\pi f d_{S,R}}{c}) + \eta_{LoS}) \\
 &+ (1 - P_{LoS})(20 \log_{10}(\frac{4\pi f d_{S,R}}{c}) + \eta_{NLoS}) \\
 &= 20 \log_{10}(d_{S,R}) + AP_{LoS}(n) + B.
 \end{aligned}
 \tag{5}$$

$A = \eta_{LoS} - \eta_{NLoS}$ and $B = 20 \log_{10}(\frac{4\pi f}{c}) + \eta_{NLoS}$. Note that η_{LoS} is always less than η_{NLoS} for any given environment [6], and thus $A < 0$ holds.

The transmission speed of the first hop link is mathematically quantized as:

$$T_1 = B_1 \log_2(1 + \frac{P_S 10^{-\frac{PL}{10}}}{B_1 N_0}).
 \tag{6}$$

P_S is the transmit power of the ground base station, and B_1 is the available bandwidth for the first hop link.

The research in this paper intends to maximize the system downlink throughput of the communication by optimizing the UAV deployment location and system resource allocation. In this context, all users shall be provided with equivalent communications by the operator company. The mathematical expression of the problem is:

$$\begin{aligned}
 &\max_{B_{2i}, B_1, P_{2i}, x_{R,i}, y_{R,i}, z_{R,i}} \sum_{i=1}^n T_{2i} && (7a) \\
 s.t. & \quad x_B \leq x_U \leq x_D && (7b) \\
 & \quad 0 \leq y_U \leq y_B && (7c) \\
 & \quad 0 \leq z_U \leq z_B && (7d) \\
 & \quad B_1 \geq 0, B_{2i} \geq 0, \forall i && (7e) \\
 & \quad \sum_{i=1}^n B_{2i} + B_1 \leq B_{max} && (7f) \\
 & \quad P_{2i} \geq 0, \forall i && (7g) \\
 & \quad \sum_{i=1}^n P_{2i} \leq P_{max} && (7h) \\
 & \quad T_{2i} = T_{2j} = \dots = T_{2n} && (7i) \\
 & \quad \sum_{i=1}^n T_{2i} \leq T_1 && (7j)
 \end{aligned}$$

Here, (7b), (7c) and (7d) initially limit the deployment range of UAVs, but only in this range, in order to reduce the communication elevation of UAVs and further reduce the signal through-wall loss in the second hop connection. For example, if $z_U > z_B$, it is likely to increase the communication elevation of a large number of second hop links. The expressions (7e) and (7g) represent the non-negative requirements for resource allocation. Expression (7f) represents the total bandwidth limit. Expression (7h) means that the total available transmit power for the second hop link should not exceed the maximum transmit power (P_{max}) of the UAV's relay. Expression (7i) reflects the fairness of the two-hop communication system. All users' lives are equal, and they should receive the same communication services. Expression (7j) is the causal constraint of information. The speed and content of the second hop link should not be greater than those of the first hop.

3. Algorithm Design

We need to transform the equality constraints in problem (7) into inequality constraints. Then, we decompose the transformed problem into two sub-problems: location

optimization and resource optimization. Resource optimization includes bandwidth and power optimization. Finally, we propose a joint optimization algorithm to jointly optimize the two sub-problems.

3.1. Problem Reformulation

In order to further process the information causality constraint (7j), we add a controllable relaxation variable Γ to the original problem. After equivalent deformation, the original problem (7) is rewritten as:

$$\max_{B_{2i}, B_1, P_i, x_R, y_R, z_R, \Gamma} \Gamma \quad (8a)$$

$$s.t. \quad (7b), (7c), (7d), (7e), (7f), (7g), (7h), (7i), \quad (8b)$$

$$\Gamma \leq \sum_{i=1}^n T_{2i}, \quad (8c)$$

$$\Gamma \leq T_1. \quad (8d)$$

In order to further calculate the user fairness constraint (7i), we add a new definition, $\Omega = \min\{T_{2i}, T_j, \dots, T_n\}$, and problem (8) is equivalently transformed and a new representation is obtained:

$$\max_{B_{2i}, B_1, P_i, x_R, y_R, z_R, \Gamma, \Omega} \Gamma \quad (9a)$$

$$s.t. \quad (7b), (7c), (7d), (7e), (7f), (7g), (7h), (8d), \quad (9b)$$

$$\Gamma \leq n\Omega, \quad (9c)$$

$$\Omega \leq T_{2i}, \forall i. \quad (9d)$$

3.2. Location Sub-Problem

In this section, the resource allocation is fixed, and the problem (9) is simplified into the location optimization sub-problem:

$$\max_{x_R, y_R, z_R, \Gamma, \Omega} \Gamma \quad (10a)$$

$$s.t. \quad (7b), (7c), (7d), (8d), (9c), (9d). \quad (10b)$$

Although the resource is fixed at this time, (10) is still a non-convex problem. This is due to the complexity of the fading model. In short, (8d) and (9d) in the constraint conditions make (10) unable to obtain a feasible region with concave or convex properties. Next, we need to convert the non-convex feasible region into a convex feasible region. In this process, we need to use the CVX toolkit in MATLAB [24].

To solve this problem, we introduce the relaxation variable Q_1 (the same form of relaxation variable Q_k as in the following of the paper, where k represents the index of the relaxation variable) and make an equivalent transformation of (8d):

$$\Gamma \leq B_1 \log_2 \left(1 + \frac{P_S Q_1}{B_1 N_0} \right), \quad (11)$$

$$\ln Q_1 + \frac{\ln 10}{10} PL \leq 0. \quad (12)$$

To further simplify constraint (12), it is once again transformed as follows:

$$\ln Q_1 + 2 \ln(d_{S,R}) + \frac{A \ln 10}{10 Q_2} + \frac{B \ln 10}{10} \leq 0, \quad (13)$$

$$Q_2 \geq 1 + a_0 \exp[Q_3], \tag{14}$$

$$Q_3 \geq -b_0 \left(\frac{180}{\pi} \tan^{-1} \left(\frac{1}{Q_4} \right) - a_0 \right), \tag{15}$$

$$\ln Q_4 + \ln(z_R - z_S) \geq \ln d_H. \tag{16}$$

We find that constraints (13), (15) and (16) are non-convex, but they can be handled efficiently by using the SCA method [25]. Regarding $\ln Q_1$ of constraint (13), its convex upper bound can be obtained using a first-order Taylor expansion:

$$\ln Q_1 \leq \ln Q_1^l + \frac{Q_1 - Q_1^l}{Q_1^l} = f_{Q_1}^{up}. \tag{17}$$

Similarly, the convex upper bound of $\ln(d_{S,R})$ can be written as follows:

$$\ln d_{S,R} \leq \ln d_{S,R}^l + \frac{d_{S,R} - d_{S,R}^l}{d_{S,R}^l} = f_{x_R, y_R, z_R}^{up}, \tag{18}$$

where $d_{S,R}^l = \sqrt{(x_S - x_R^l)^2 + (y_S - y_R^l)^2 + (z_S - z_R^l)^2}$. The convex upper bound of $\ln(d_H)$ (represented by f_{x_R, y_R}^{up}) in constraint (16) has the same form as $\ln d_{S,R}$, and thus is omitted. Moreover, since $A \leq 0$, the convex upper bound of $\frac{A}{Q_2}$ can be written as follows:

$$\frac{A}{Q_2} \leq \frac{A}{Q_2^l} - \frac{A(Q_2 - Q_2^l)}{(Q_2^l)^2} = f_{Q_2}^{up}. \tag{19}$$

For constraint (15), the concave lower bound of $\tan^{-1}(\frac{1}{Q_4})$ can be calculated as follows:

$$\tan^{-1} \left(\frac{1}{Q_4} \right) \geq \tan^{-1} \left(\frac{1}{Q_4^l} \right) - \frac{Q_4 - Q_4^l}{1 + (Q_4^l)^2} = f_{Q_4}^{low}. \tag{20}$$

We make an equivalent transformation of (9d):

$$\Omega \leq B_{2i} \log_2 \left(1 + \frac{P_{2i} \Xi_i}{B_{2i} N_0} \right), \forall i, \tag{21}$$

$$\ln \Xi_i + \frac{\ln 10}{10} (PL_{Fi} + \beta_1 + \beta_2 (1 - \omega_i)^2 + PL_{Ii}) \leq 0, \forall i, \tag{22}$$

$$\ln \omega_i + \ln d_{R, D_i} \leq \ln(x_R - x_B), \forall i. \tag{23}$$

It is easy to observe that the convex upper bound for $\ln \Xi_i$ (represented by $f_{\ln \Xi_i}^{upper}$), PL_{Fi} (represented by $f_{PL_{Fi}}^{upper}$), $\ln \omega_i$ (represented by $f_{\ln \omega_i}^{upper}$) and $\ln d_{R, D_i}$ (represented by $f_{\ln d_{R, D_i}}^{upper}$) has a similar form as that used in (17); thus, it is also omitted.

By using the above relaxation constraints and boundaries, we only need to use CVX to solve problem (24), and problem (10) will be solved.

$$\begin{aligned} & \max_{x_R, y_R, z_R, \Gamma, \Omega, \Xi_i, \omega_i, Q_1, Q_2, Q_3, Q_4} \Gamma & (24a) \\ \text{s.t. } & (7b), (7c), (7d), (9c), (11), (14), (21) & (24b) \\ & f_{Q_1}^{up} + 2f_{x_R, y_R, z_R}^{up} + \frac{\ln 10}{10} f_{Q_2}^{up} + \frac{B \ln 10}{10} \leq 0, & (24c) \\ & Q_3 \geq -b_0 \left(\frac{180}{\pi} f_{Q_4}^{low} - a_0 \right), & (24d) \\ & \ln Q_4 + \ln(z_R - z_S) \geq f_{x_R, y_R}^{up}, & (24e) \\ & f_{\ln \Xi_i}^{upper} + \frac{\ln 10}{10} (f_{PLFi}^{upper} + \beta_1 + \beta_2(1 - \omega_i)^2 + PL_{Ii}) \leq 0, \forall i, & (24f) \\ & f_{\ln \omega_i}^{upper} + f_{\ln d_{R, D_i}}^{upper} \leq \ln(x_R - x_B), \forall i. & (24g) \end{aligned}$$

3.3. Resource Allocation Sub-Problem

In this section, the UAV’s location is fixed, and problem (9) is simplified to a resource allocation sub-problem:

$$\begin{aligned} & \max_{B_{2i}, B_1, P_i, \Gamma, \Omega} \Gamma & (25a) \\ \text{s.t. } & (7e), (7f), (7g), (7h), (8d), (9c), (9d). & (25b) \end{aligned}$$

Constraint (9d) is non-convex, which leads to the non-convex problem (25). Moreover, constraint (8d) is convex, but it has a complicated form, which means that the CVX cannot be applied to handle it.

To efficiently solve the above problem, constraint (8d) is transformed as follows:

$$\ln \Gamma \leq \ln B_1 + \ln Q_5, \tag{26}$$

$$Q_5 \leq \log_2(P_5 10^{-\frac{PL}{10}} + B_1 N_0) - \log_2(B_1 N_0). \tag{27}$$

Furthermore, constraint (9d) is transformed as:

$$\ln \Gamma \leq \ln B_{2i} + \ln Q_{6i}, \forall i, \tag{28}$$

$$Q_{6i} \leq \log_2(1 + Q_{7i} 10^{-\frac{PL_i}{10}}), \forall i, \tag{29}$$

$$\ln Q_{7i} \leq \ln P_i - \ln(B_i N_0), \forall i. \tag{30}$$

In the above non-convex constraints (26), (27), (28) and (30), the slack bound also has the same form as that used in (17). For brevity, we only denote the convex upper bounds of $\ln \Gamma$, $\log_2(B_1 N_0)$, $\ln Q_{7i}$ and $\ln(B_i N_0)$ as $f_{\ln \Gamma}^{upper}$, $f_{\log_2(B_1 N_0)}^{upper}$, $f_{\ln Q_{7i}}^{upper}$ and $f_{\ln(B_i N_0)}^{upper}$, respectively.

Consequently, the (l)-th iteration of the SCA for problem (25) is changed to solve the following standard convex problem using CVX:

$$\begin{aligned} & \max_{B_{2i}, B_1, P_i, \Gamma, \Omega} \Gamma & (31a) \\ \text{s.t. } & (7e), (7f), (7g), (7h), (9c), (29) & (31b) \\ & f_{\ln \Gamma}^{upper} \leq \ln B_1 + \ln Q_5, & (31c) \\ & Q_5 \leq \log_2(P_5 10^{-\frac{PL}{10}} + B_1 N_0) - f_{\log_2(B_1 N_0)}^{upper} & (31d) \\ & f_{\ln \Gamma}^{upper} \leq \ln B_{2i} + \ln Q_{6i}, \forall i, & (31e) \\ & f_{\ln Q_{7i}}^{upper} \leq \ln P_i - f_{\ln(B_i N_0)}^{upper}, \forall i. & (31f) \end{aligned}$$

3.4. JLRO Algorithm

In this section, we provide our proposed joint optimization algorithm, as shown in the JLRO algorithm. Algorithm 1 will iterate several times for the location sub-problem and the resource allocation sub-problem until it converges.

In step 1 of the JLRO algorithm, set $l = 0$ means that at the beginning of the SCA, the input used to obtain the bounded constraints needs to be initialized. In step 8 of the JLRO algorithm, the convergence condition adopts the following principle:

$$\frac{\Gamma^{l+1} - \Gamma^l}{\Gamma^l} \leq \delta. \tag{32}$$

where δ represents the convergence threshold, which can be set as needed. The total complexity of the JLRO algorithm is in the order of $O(N_{var}N_{con})$, where N_{con} is the iteration number for convergence. The following simulation results will further prove that our algorithm has good convergence.

Algorithm 1: JLRO

1. Set $l = 0$. Initialize $\mathbf{var}_{24}^0 = \{x_R^0, y_R^0, z_R^0, Q_1^0, Q_2^0, Q_4^0, \Xi_i^0, \omega_i^0\}$ and $\mathbf{var}_{31}^0 = \{\Gamma^0, B_1^0, Q_{7i}^0, B_i^0\}$;
 2. Repeat
 3. Solve problem (24) with given P_i, B_{2i}, B_1 and \mathbf{var}_{24}^l , and obtain the solution \mathbf{var}_{24}^{l+1} ;
 4. Solve problem (31) with given $x_R^{l+1}, y_R^{l+1}, z_R^{l+1}$ and \mathbf{var}_{31}^l , and obtain the solution \mathbf{var}_{31}^{l+1} ;
 5. Update $l = l + 1$;
 6. Until
 7. Reach convergence condition.
-

4. Simulation Results

We provide the parameters that may be used in the simulation experiment. Unless otherwise stated, the parameters in Tables 1 and 2 are used. Table 3 shows the propagation parameters in different environments. The simulation in this article was conducted in the environment of Dense City. The coordinate information for 10 indoor users is shown in Table 4. These coordinates are the same as those in document [1]. These coordinates have no particularity. The handheld terminal is 1.5 m above the ground.

Table 1. Notations and definitions.

Notation	Definition
$S(x_S, y_S, z_S)$	The coordinates of the signal transmitter
$R(x_R, y_R, z_R)$	The coordinates of the UAV relay
$D_i(x_i, y_i, z_i)$	The coordinates of the i -th indoor user
$d_{S,R}$	The linear distance between the BS and the UAV
d_{R,D_i}	The linear distance between the UAV and the exterior wall of the building
d_i	The indoor transmission distance of the i -th indoor user
θ	The elevation angle of signal passing through the wall
x_B, y_B, z_B	The length, width and height of building (B)
T_{2i}	The transmission speed of the i -th user in the second hop link
P_{2i}	The power allocated by the UAV to the i -th user

Table 1. Cont.

Notation	Definition
B_{2i}	The bandwidth allocated by the UAV to the i -th user
N_0	The noise power spectral density
P_{LoS}	The LOS probability
a_0, b_0	The environment-related constants
η_{LoS}	The supplementary path loss for the LOS channel
η_{NLoS}	The supplementary path loss for the NLOS channel
T_1	The transmission speed of the first hop link
PL	The first hop path loss
P_S	The transmit power of the ground base station
B_1	The available bandwidth for the first hop link
PL_{2i}	The second hop path loss of the i -th user
PL_{Fi}	The outdoor transmission loss of the i -th user in the second hop link
PL_{Bi}	The wall transmission loss of the i -th user in the second hop link
PL_{Ii}	The indoor transmission loss of the i -th user in the second hop link
c	The speed of light
f	The carrier frequency used for the signal
$\beta_1, \beta_2, \beta_3$	ITU standard data
P_{max}	The maximum transmit power of the UAV relay
B_{max}	The maximum bandwidth of the system

Table 2. Simulation parameters.

Length, width and height of building	20 m, 50 m, 100 m
Coordinate of the ground BS	(1000, 25, 30)
Carrier frequency: f	1 GHz
Noise power spectral density: N_0	-174 dbm/Hz
Maximum total system bandwidth: B_{max}	1 MHz
Maximum total system transmission power: P_{max}	1 w
Transmission power of the BS: P_1	0.5 w
Convergence error: δ	10^{-3}

Table 3. Propagation parameters in different environments.

Different Environments	$a_0, b_0, \eta_{LoS}, \eta_{NLoS}$
Suburb	(4.88, 0.43, 0.1, 21)
City	(9.61, 0.16, 1, 20)
Dense city	(12.08, 0.11, 1.6, 23)
High-rise building city	(27.23, 0.08, 2.3, 34)

Table 4. The coordinates of indoor users.

S_1	S_2	S_3	S_4	S_5
(12, 21, 91.5)	(8, 35, 43.5)	(1, 48, 76.5)	(17, 42, 55.5)	(8, 38, 25.5)
S_6	S_7	S_8	S_9	S_{10}
(9, 5, 82.5)	(5, 9, 16.5)	(17, 15, 4.5)	(12, 25, 31.5)	(14, 17, 67.5)

Figure 2 shows the convergence of the proposed JLRO algorithm. The markers “40In”, “30In”, “20In”, “10In” and “5In” indicate that the number of indoor users is 40, 30, 20, 10 and 5, respectively. The marker “5In” uses the five user coordinates in the first row of Table 4; “10In” uses the ten user coordinates in Table 4. There are 10 user coordinates in “20In”, “30In” and “40In”, as seen in Table 4, and the rest are randomly generated user coordinates. All user coordinates have no particularity. As can be seen from Figure 2, the proposed algorithm can achieve convergence within six iterations. When the throughput reaches a steady state, the algorithm converges. Based on the premise that there is a certain total bandwidth and total transmission power, the total throughput of the system increases gradually with the increase in users. However, the increase reduces over time. When the number of users increases to a certain threshold, the total throughput tends towards stability. When the number of users increases from 30 to 40, the throughput increase is small, or even considered not to increase. This is directly related to the influence of bandwidth on noise power.

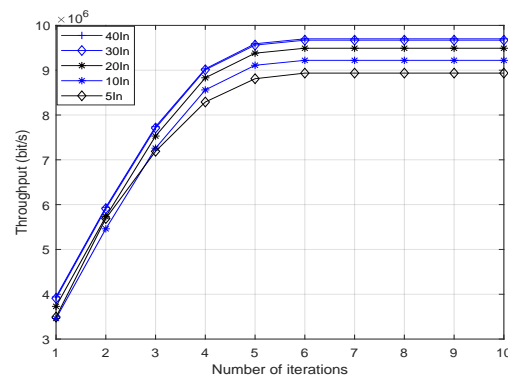
**Figure 2.** Convergence of JLRO algorithm with different numbers of users.

Figure 3 shows the user deployment and time-sharing deployment of the UAV. Figure 3a shows the user coordinates in Table 4, which are represented by “ $D1 \sim D10$ ”. R indicates the deployment location of the UAV when the users are distributed. The deployment coordinates of the UAV are (48.6, 23.2, 55.8). Users have profit-driven mobility. Therefore, the UAV needs to update its deployment location according to the user’s movements in real time. Figure 3b shows the deployment location of the UAV when it moves with the user. Each second, the user will report the current location information to the UAV, and the UAV will move in response. “ $t1 \sim t10$ ” indicates the location of the UAV every second. The location at time $t1$ is the same as that of R in Figure 3a. Of course, what we perform is location deployment, not trajectory optimization. The proposed algorithm can only provide the final deployment location of the UAV, and the moving trajectory is not our research focus. If the deployment interval is regarded as infinitesimal, it will be trajectory optimization, but the current computing power of UAVs cannot meet this.

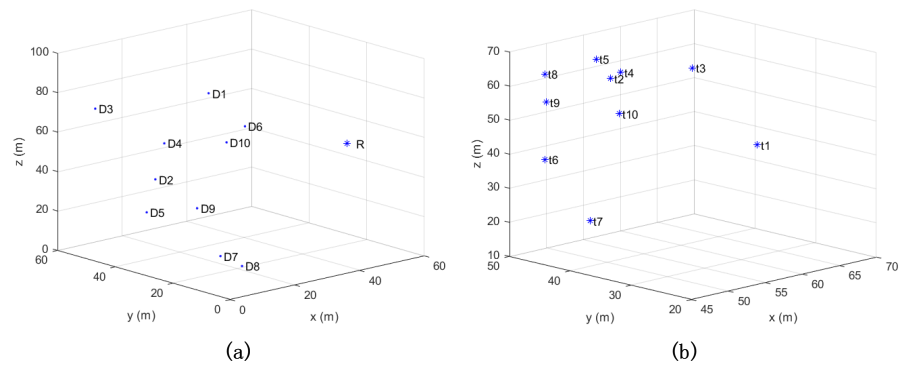


Figure 3. User deployment and UAV time-sharing deployment. (a) user coordinates in Table 4; (b) the deployment location of the UAV when it moves with the user.

Figure 4 shows the fairness of the second hop link. The number of indoor users used in this simulation result is 10, and the user coordinates are from Table 4. The blue column represents the JLRO algorithm, and the red column represents the algorithm without considering fairness. The results show that the JLRO algorithm can ensure the fairness of users. The throughput of each user is 9.22×10^5 bit/s. The non-public balance law cannot guarantee the fairness of public households. Among them, the throughput of several channels is particularly high, while the throughput of the remaining channels can only meet the most basic communication requirements. The most basic communication requirement we set is 4×10^5 bit/s. Especially for the second channel, the throughput is particularly high. This is because the loss of the channel is the smallest. The system allocates more bandwidth and power to it, which can bring higher system benefits. However, with the increase in power and bandwidth, this benefit will become increasingly smaller. When the revenue of the seventh channel is higher than that of the second channel, the system will fairly allocate the remaining bandwidth to the seventh channel. This is also the reason for the high throughput of the seventh channel. This continues until all resources are used by the system. The results also show that the sum of throughput of the red column is greater than that of the blue column. This means that the system’s fairness comes at the cost of losing part of the throughput.

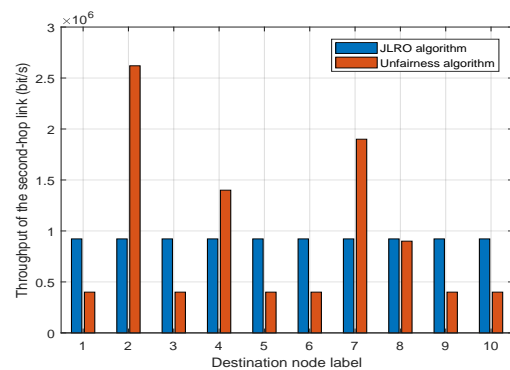


Figure 4. Fairness of the second hop link.

Figure 5 shows that the bandwidth allocation changes with the increase in B_{max} . The results show that the allocated bandwidth of the first hop link is significantly higher than that of the second hop link. This is because the transmission distance of the first hop link is much higher than that of the second hop link. Although the loss of signal passing through the wall is great, the loss caused by long distances is even greater. With the growth of B_{max} , the bandwidth of each hop link increases, but not linearly because there is a convolution between bandwidth and power. When B_{max} becomes bigger and bigger, the bandwidth required for the first hop link increases faster. We note that the bandwidth allocation of

$D2$ is minimal. This is consistent with the conclusion that the throughput of the second channel is the largest when fairness is not considered, as shown in Figure 4, because the loss of the second channel is the smallest.

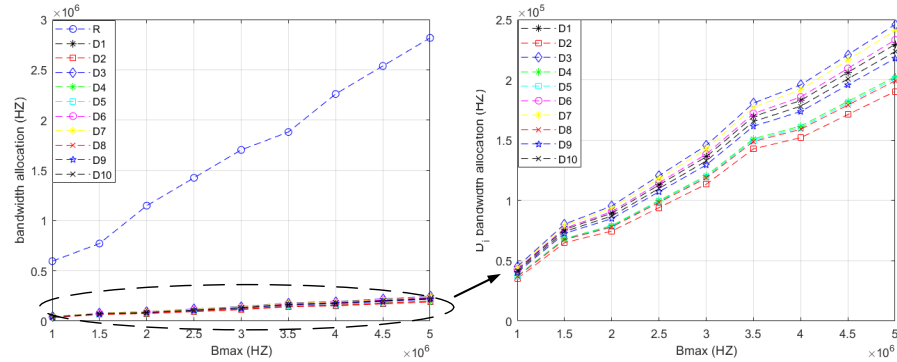


Figure 5. System bandwidth allocation.

Figure 6 shows that the power distribution changes with an increase in P_{max} . Obviously, with the increase in P , the transmission power of each link increases. However, the increasing trend is not linear because there is a convolutional relationship between power and bandwidth. This is consistent with the conclusion shown in Figure 5. Further observation shows that the transmission power required by $D2$ is the lowest. This is similar to the bandwidth requirements of $D2$ in Figure 4. The reason is that the path loss of $D2$ is small, and the demand for bandwidth and power is small.

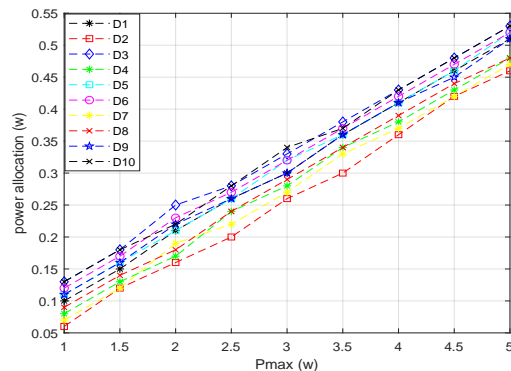


Figure 6. System power allocation.

Figure 7 shows the relationship between UAV deployment coordinates and x_D . With the increase in x_D , x_U increases gradually, but the increase range is not large and decreases over time. The increase in x_U is due to the increase in the total transmission distance. The reason for the small increase is that the indoor propagation loss increases too much, which will seriously reduce the throughput of the second hop link and then affect the system throughput. The increase in x_D has little effect on y_U and z_U , which can almost be ignored because the most important factor affecting y_U and z_U is the coordinates of indoor users.

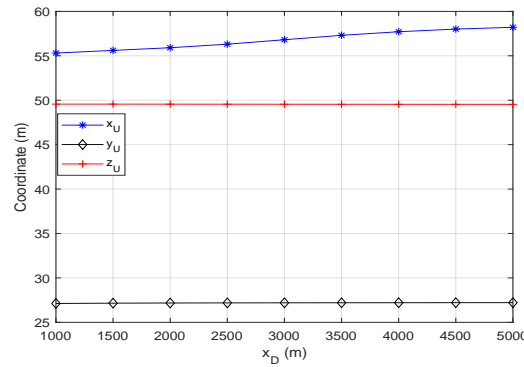


Figure 7. Relationship between UAV deployment coordinates and x_D .

Figure 8 shows the effect of x_D on power, bandwidth and throughput. Figure 8a shows the effect of x_D on bandwidth allocation. With the growth of x_D , the bandwidth resources of the first hop link gradually increase. The increased bandwidth resources are mainly used to make up for the increased loss caused by distance. The bandwidth resources of the second hop link are gradually reduced. Figure 8b shows the effect of x_D on power distribution. We find that the effect of x_D on power allocation is very small and almost negligible. This is because the power allocation only exists in the second hop link, independent of the distance of the first hop link. Moreover, as can be seen from Figure 7, although x_D has an impact on the linear distance of the second hop link, it is a small impact. As shown in Figure 8c, the throughput of reasoning will decrease, which is consistent with the above two phenomena.

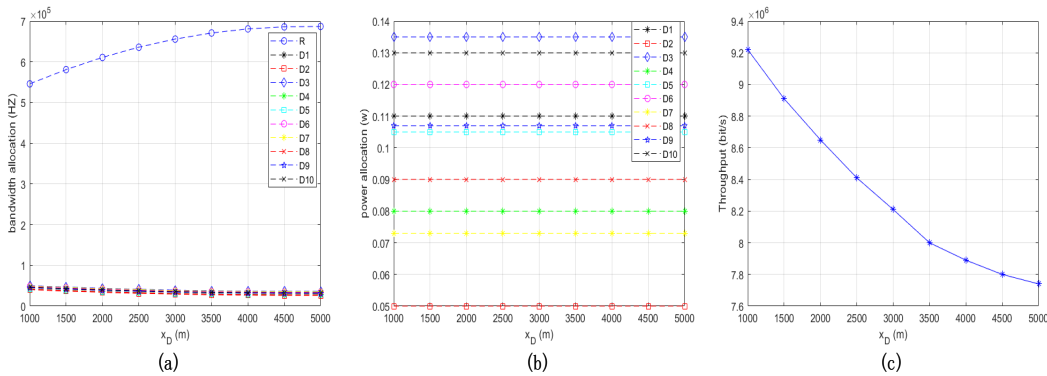


Figure 8. Impact of x_D on power, bandwidth and throughput. (a) the effect of x_D on bandwidth allocation; (b) the effect of x_D on power distribution; (c) the throughput of reasoning.

Figure 9 presents a comparison between our proposed algorithm and two benchmark algorithms based on random locations. Figure 9a shows the comparison between the JLRO algorithm and the benchmark of the bandwidth allocated at a fixed total power and random location of the UAV (labeled 'BA benchmark'), which fixed $P_{max} = 1W$; the total bandwidth B_{max} increases and the throughput increases gradually. However, as the total bandwidth increases, the increase in throughput diminishes. This is because, in formulas (3) and (6) of the Shannon formula, an increase in B leads to an increase in noise power. A random location means that the deployment location of the UAV is random, but the power and bandwidth allocations are still optimized according to the JLRO algorithm. At $B_{max} = 4.5$ Mhz, the random deployment location of the UAV is very close to the location computed by JLRO, so the throughput coordinates of the two points are very close. Similarly, Figure 9b depicts the comparison between the JLRO algorithm and the benchmark of power optimized at a fixed total bandwidth and random location of the UAV (labeled 'PO benchmark'), with the fixed bandwidth $B_{max} = 1$ Mhz.

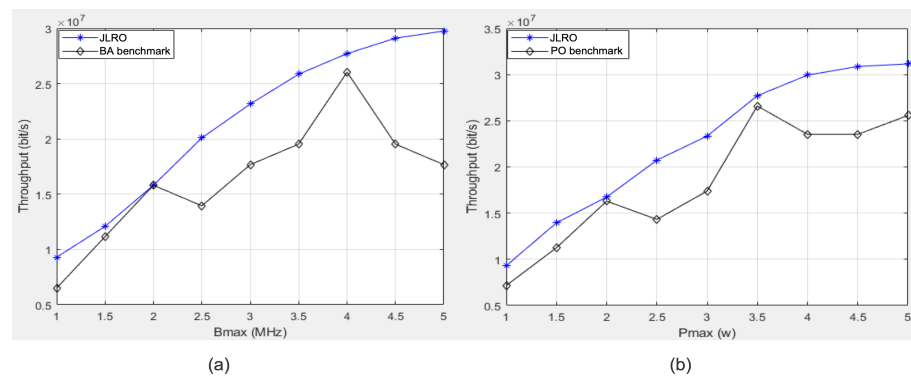


Figure 9. Performance comparison between the proposed JLRO algorithm and benchmark algorithms. (a) the comparison between the JLRO algorithm and the benchmark of the bandwidth allocated at a fixed total power and random location of the UAV; (b) the comparison between the JLRO algorithm and the benchmark of power optimized at a fixed total bandwidth and random location of the UAV.

5. Conclusions

In this paper, a UAV is used as an air relay to build a two-hop relay link between indoor users and ground base stations. This paper constructed a two-hop downlink throughput maximization problem based on the UAV's location and resource allocation while ensuring user fairness. We quantify this problem as a mathematical problem; however, it is non-convex. In order to effectively solve the non-convex problem, we first transformed it into a convex problem and proposed the JLRO algorithm to jointly optimize location optimization and resource allocation. We also analyzed the impact of user location information and bandwidth and power changes on the UAV's location and system throughput. The simulation results show that the JLRO algorithm can ensure that the system will have maximum throughput and good convergence performance under the premise of user fairness. The simulation results also indicate that our proposed algorithm outperforms the benchmarks.

Author Contributions: Z.G.: Formal analysis, Methodology, Writing—original draft, Writing-review & editing; B.H.: Supervision, Resources, Conceptualization, review & editing; S.C.: Funding support, Supervision, Conceptualization. All authors have read and agreed to the published version of the manuscript.

Funding: This work was supported by the National Natural Science Foundation of China (NSFC) under grant 61931005, and the National Key R&D Program of China under Grant 2020YFB1807900.

Data Availability Statement: The data are available from the corresponding author on reasonable request.

Conflicts of Interest: The authors declare no conflict of interest.

Abbreviations

UAV	Unmanned aerial vehicle
JLRO	Joint UAV location deployment and resource allocation optimize
ATG	Air to ground
WPCN	Wireless powered communication network
SCA	Successive convex approximation
LOS	Line of sight

References

1. Feng, W.; Tang, J.; Yu, Y.; Song, J.; Zhao, N.; Chen, G.; Wong, K.K.; Chambers, J. UAV-Enabled SWIPT in IoT Networks for Emergency Communications. *IEEE Wirel. Commun.* **2020**, *27*, 140–147. [[CrossRef](#)]
2. Chang, B.; Tang, W.; Yan, X.; Tong, X.; Chen, Z. Integrated Scheduling of Sensing, Communication, and Control for mmWave/THz Communications in Cellular Connected UAV Networks. *IEEE J. Sel. Areas Commun.* **2022**, *40*, 2103–2113. [[CrossRef](#)]

3. Wang, B.; Sun, Y.; Sun, Z.; Nguyen, L.D.; Duong, T.Q. UAV-Assisted Emergency Communications in Social IoT: A Dynamic Hypergraph Coloring Approach. *IEEE Internet Things J.* **2020**, *7*, 7663–7677. [[CrossRef](#)]
4. Bekkouche, O.; Samdanis, K.; Bagaa, M.; Taleb, T. A Service-Based Architecture for Enabling UAV Enhanced Network Services. *IEEE Netw.* **2020**, *34*, 328–335. [[CrossRef](#)]
5. Jiang, B.; Yang, J.; Xu, H.; Song, H.; Zheng, G. Multimedia Data Throughput Maximization in Internet-of-Things System Based on Optimization of Cache-Enabled UAV. *IEEE Internet Things J.* **2019**, *6*, 3525–3532. [[CrossRef](#)]
6. Al-Hourani, A.; Kandeepan, S.; Lardner, S. Optimal LAP Altitude for Maximum Coverage. *IEEE Wirel. Commun. Lett.* **2014**, *3*, 569–572. [[CrossRef](#)]
7. Rahman, S.u.; Kim, G.-H.; Cho, Y.-Z.; Khan, A. Positioning of UAVs for throughput maximization in software-defined disaster area UAV communication networks. *J. Commun. Netw.* **2018**, *20*, 452–463. [[CrossRef](#)]
8. Wu, Q.; Zhang, R. Common Throughput Maximization in UAV-Enabled OFDMA Systems with Delay Consideration. *IEEE Trans. Commun.* **2018**, *66*, 6614–6627. [[CrossRef](#)]
9. Miao, J.; Wang, P.; Zhang, Q.; Wang, Y. Throughput maximization for multi-UAV enabled millimeter wave WPCN: Joint time and power allocation. *China Commun.* **2020**, *17*, 142–156. [[CrossRef](#)]
10. Lee, J.-H.; Park, K.-H.; Ko, Y.-C.; Alouini, M.-S. Throughput Maximization of Mixed FSO/RF UAV-Aided Mobile Relaying with a Buffer. *IEEE Trans. Wirel. Commun.* **2021**, *20*, 683–694. [[CrossRef](#)]
11. Wang, Z.; Liu, R.; Liu, Q.; Han, L.; Wu, Y.; Thompson, J.S. QoS-Oriented Sensing–Communication–Control Co-Design for UAV-Enabled Positioning. *IEEE Trans. Green Commun. Netw.* **2023**, *7*, 497–511. [[CrossRef](#)]
12. Wang, Y.; Chen, M.; Pan, C.; Wang, K.; Pan, Y. Joint Optimization of UAV Trajectory and Sensor Uploading Powers for UAV-Assisted Data Collection in Wireless Sensor Networks. *IEEE Internet Things J.* **2022**, *9*, 11214–11226. [[CrossRef](#)]
13. Shakhathreh, H.; Khreishah, A.; Khalil, I. Indoor Mobile Coverage Problem Using UAVs. *IEEE Syst. J.* **2018**, *12*, 3837–3848. [[CrossRef](#)]
14. Cui, J.; Hu, B.; Chen, S. Resource allocation and location decision of a UAV-relay for reliable emergency indoor communication. *Comput. Commun.* **2020**, *159*, 15–25. [[CrossRef](#)]
15. Sheikh, M.U.; Hiltunen, K.; Lempiäinen, J. Angular wall loss model and Extended Building Penetration model for outdoor to indoor propagation. In Proceedings of the 2017 13th International Wireless Communications and Mobile Computing Conference (IWCMC), Valencia, Spain, 26–30 June 2017; pp. 1291–1296. [[CrossRef](#)]
16. Cui, J.; Hu, B.; Chen, S. A decision-making scheme for UAV maximizes coverage of emergency indoor and outdoor users. *Ad Hoc Netw.* **2021**, *112*, 102391. [[CrossRef](#)]
17. Xie, L.; Xu, J.; Zhang, R. Throughput Maximization for UAV-Enabled Wireless Powered Communication Networks. *IEEE Internet Things J.* **2019**, *6*, 1690–1703. [[CrossRef](#)]
18. Hua, M.; Yang, L.; Wu, Q.; Swindlehurst, A.L. 3D UAV Trajectory and Communication Design for Simultaneous Uplink and Downlink Transmission. *IEEE Trans. Commun.* **2020**, *68*, 5908–5923. [[CrossRef](#)]
19. Kang, J.; Kashihara, H.; Sumantyo, J.T.S.; Kim, J.-H. Performance Analysis of Uplink NOMA based Full-Duplex UAV for Indoor Disaster Environment. In Proceedings of the 2021 International Conference on Information and Communication Technology Convergence (ICTC), Jeju Island, Republic of Korea, 20–22 October 2021; pp. 245–247. [[CrossRef](#)]
20. Xie, L.; Xu, J.; Zeng, Y. Common Throughput Maximization for UAV-Enabled Interference Channel with Wireless Powered Communications. *IEEE Trans. Commun.* **2020**, *68*, 3197–3212. [[CrossRef](#)]
21. Liu, T.; Cui, M.; Zhang, G.; Wu, Q.; Chu, X.; Zhang, J. 3D Trajectory and Transmit Power Optimization for UAV-Enabled Multi-Link Relaying Systems. *IEEE Trans. Green Commun. Netw.* **2021**, *5*, 392–405. [[CrossRef](#)]
22. Li, Z.; Zhao, X.; Hu, F.; Zhao, Z.; Villacrés, J.L.C.; Braun, T. SoICP: A Seamless Outdoor–Indoor Crowdsensing Positioning System. *IEEE Internet Things J.* **2019**, *6*, 8626–8644. [[CrossRef](#)]
23. Series, M. Guidelines for evaluation of radio interface technologies for imt-advanced. *Report ITU* **2009**, 638. Available online: <https://www.itu.int/pub/R-REP-M.2135-1-2009> (accessed on 21 July 2020).
24. CVX RESEARCH. CVX: Matlab Software for Disciplined Convex Programming. Available online: <http://cvxr.com/cvx/> (accessed on 21 July 2020).
25. Palomar, D.P. Algorithms: Successive Convex Approximation (SCA). Available online: https://palomar.home.ece.ust.hk/ELEC5470_lectures/slides_algorithms_SCA.pdf (accessed on 21 July 2020).

Disclaimer/Publisher’s Note: The statements, opinions and data contained in all publications are solely those of the individual author(s) and contributor(s) and not of MDPI and/or the editor(s). MDPI and/or the editor(s) disclaim responsibility for any injury to people or property resulting from any ideas, methods, instructions or products referred to in the content.